metals

MDPI

Article

The Impact of EMS on the Temperature Fluctuations, Appearance, and Microstructure of GTA Stainless Steel Welds

Sheng-Long Jeng *, Dai-Ping Su, Jing-Ting Lee and Jiunn-Yuan Huang

Nuclear Fuels and Materials Division, Institute of Nuclear Energy Research, Taoyuan 32546, Taiwan; dpsu@iner.gov.tw (D.-P.S.); jtlee@iner.gov.tw (J.-T.L.); jyhuang@iner.gov.tw (J.-Y.H.)

* Correspondence: sljeng@iner.gov.tw; Tel.: +886-3-471-1400 (ext. 6726)

Received: 30 October 2019; Accepted: 6 January 2020; Published: 13 January 2020

Abstract: The purpose of this study was to evaluate the temperature fluctuation induced by electromagnetic stirring (EMS) and to investigate the influence of temperature fluctuation on the appearance and microstructure of the stainless steel welds. CF8A and 308L were used for the base metal and weld metal, respectively. Bead-on-plate welding (BOP) was conducted with a linear welding machine of gas tungsten arc welding (GTAW) with EMS. The experimental results show that EMS could prompt temperature alteration rates (TARs) to fluctuate between positive and negative, and enlarge the max/min ratios. Smaller ripples and surface roughness would be induced on the welds, while the dilution and the depth-to-width ratios both decreased. As a result, the ferritic and austenitic grains become more isotropic and their grain sizes become smaller.

Keywords: electromagnetic stirring (EMS); stainless steel welds; bead geometry; heating rate; cooling rate; temperature alteration rate (TAR); gas tungsten arc welding (GTAW)

1. Introduction

Welding parameters are manipulated mainly to control the arc, which in turn could affect the formation of defects in welds [1,2]. The welding parameters employed could alter the microstructure-related properties such as the mechanical properites and corrosion resistance of welds [3]. Consequently, electromagnetic force in various forms has been applied to stabilize welding arcs and reduce welding defects, as a means to improve the quality of the welds by gas tungsten arc welding (GTAW) and plasma arc welding (PAW) processes [2,4–6]. The mechanical properties and corrosion resistance of weldments were improved as well [5,7–10]. Research studies on the application of electromagnetic force to gas metal arc welding and laser welding have been conducted in recent years [9,11–13].

Electromagnetic stirring (EMS) is an application of electromagnetic force, when performing arc welding, to refine the microstructure of the weld and thus to enhance its weldability [14–16]. For aluminum alloys, it could refine the grains and change the grain orientation [17–19]. For stainless-steel (SS) welds, EMS can decrease the dilution and the grain size of ferritic welds under certain conditions [14,16,20]. Recently, it was revealed that EMS could restrain the transformation of ferritic phases in the heat-affected zone (HAZ) and prompt the dense and intersectional dendrites to form in the CF8A weldments [8]. For nickel-based alloys, it can also reduce the grain size of alloy 718 and 52M welds to increase the fatigue life and improve the signal/noise ratio of non-destructive ultrasonic examination, respectively [15,17,21,22]. The primary mechanism for grain refinement by EMS could result from dendrite detachment.

Computational analysis has been made to investigate and elucidate the EMS effects on heat transfer, fluid flow, and the solidification of welding pools in terms of temperature and velocity

profiles [10,23–25]. The differences in temperature gradients, cooling rates, and solidification rates have also been evaluated experimentally. However, the relationship between the microstructure and temperature has yet to be investigated and discussed.

With the observations of the transformed austenite and the cross-sectional microstructure in the previous study [8], the temperature fluctuation is considered to be an important factor affecting the microstructure of weldments. However, there is scarce literature on this aspect. The purpose of this study was to investigate the effect of EMS on temperature fluctuation from a practical application perspective.

2. Materials and Methods

In this study, CF8A plates were used as the base metal. They were static castings to the compositions of ASTM A351 (Standard Specification for Castings, Austenitic, for Pressure-Containing Parts) and machined to the dimensions of 150.0 × 60.0 × 10.0 (mm^3) subsequently. For a study on the susceptibility to hot cracking, the sulfur content of the test specimens was increased to the upper limit. ER308L with a diameter of 0.9 mm was employed as the filler metal. Bead-on-plate (BOP) welding tests were performed with mechanical gas tungsten arc welding. Table 1 shows the compositions of the base metal and filler metal.

Table 1. Chemical compositions of the base metal and filler metal (mass%).

Metal	C	Mn	P	S	Si	Cr	Ni	Mo	Cu	Nb	Other
CF8A	0.049	0.43	0.035	0.03	0.45	18.37	8.12	0.28	0.34	-	-
308L	0.018	1.57	0.019	0.005	0.703	19.520	9.698	0.111	0.136	-	0.010

The temperature measurements inside the HAZs and the welds were taken with thermocouples. Figure 1 shows the dimensions of the weldments and the locations of the R-type thermocouples. The thermocouples were placed beneath the welding path at various depths. The temperature was registered at a frequency of 100 Hz by GRAPHTEC GL900 (Graphtec Corporation, Yokohama, Japan). On the weld surface and HAZs, the temperature measurements were taken by a high-speed radiation pyrometer, Sensortherm H316 (Sensortherm GmbH, Taunus, Germany).

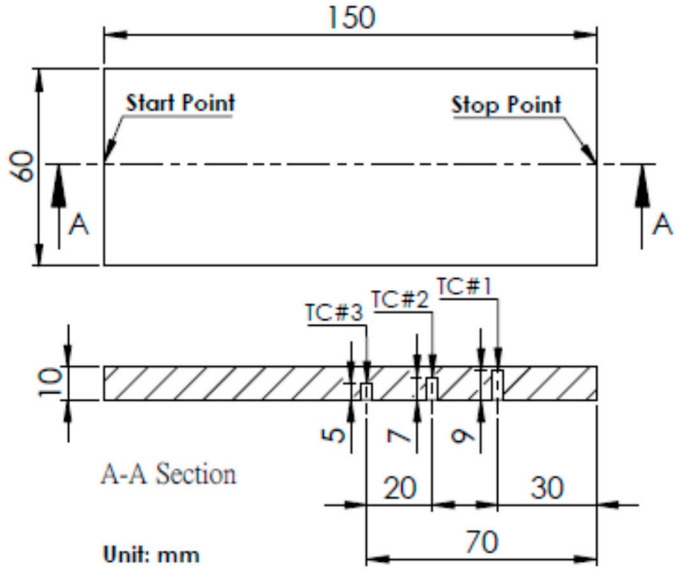

Figure 1. The dimensions of the weldments and the positions of thermal couples (TCs).

Before welding, the specimens were placed into position on a linear welding machine of GTAW (Kuang Fang Machinery Co., Ltd., Taoyuan City, Taiwan), equipped with EMS. The grooved surfaces

were cleaned with alcohol. The welding was performed under a mode of direct current electrode negative (DCEN) with 2.0% lanthanated tungsten rods of 3.2 mm in diameter. The specimens were shielded under a vaporized liquid argon with a flow rate of 25.0 SCHF (Standard Cubic Feet Per Hour). The welding current, the welding speed, and the wire feeding rate were set at 180 A, 80 mm/min, and 1000 mm/min, respectively, while the arc voltage was controlled to be at 11 V by a fixed distance between the electrode and the base metal. The EMS device (Arc Products Inc., San Diego, CA, USA) is composed of an MA-40 probe and an MP-4 controller. Its frequency was set at 3 Hz. Figure 2 depicts the EMS device and the welding machine.

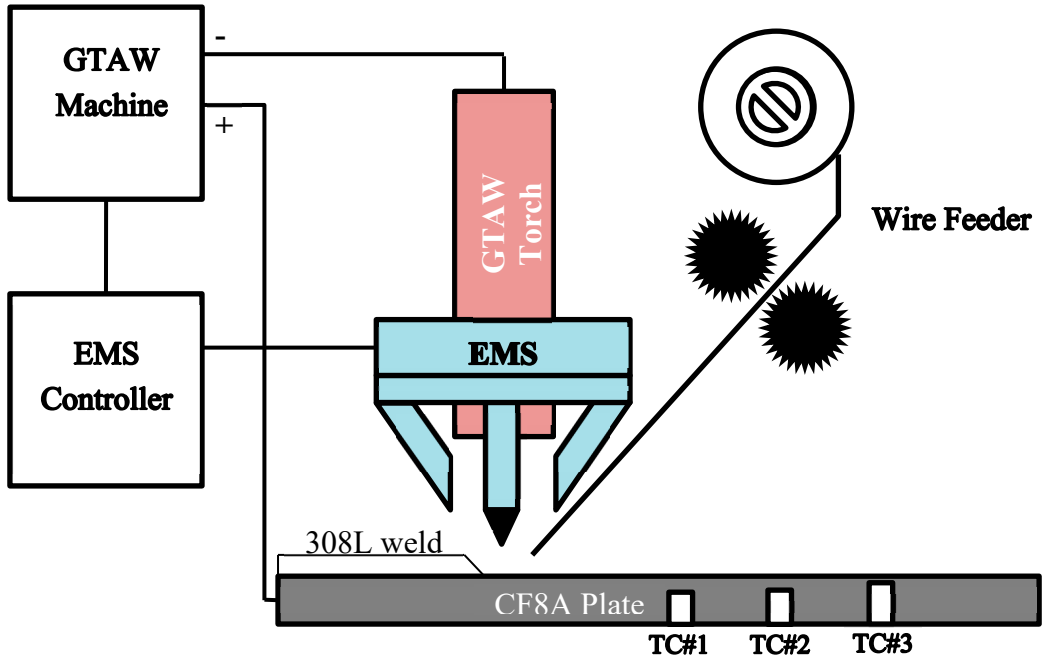

Figure 2. Schematic diagram of the experimental setup for the external electromagnetic stirring device.

The roughness and flatness of the weld surface was measured with laser confocal microscopy (Olympus, Tokyo, Japan). The specimens for microstructural observations were prepared through a series of cutting, grinding, and polishing processes. The cross-section images were taken with the aid of an optical microscope (OM). Their areas were measured with an image processing software, Image J (1.44p, National Institute of Health, Bethesda, MD, USA), to calculate the dilution ratio of welds. The phase distribution and grain orientations were investigated with a JEOL scanning electron microscope (SEM), JSM-7100F (JEOL Ltd., Tokyo, Japan), equipped with an Oxford energy-dispersive spectroscope (EDS) and an electron backscatter diffraction (EBSD) system.

3. Results

3.1. Weld Surface

Figure 3 presents the appearance of GTAW and GTAW + EMS welds. It reveals that the patterns of ripples on the GTAW weld change periodically, but that those on the GTAW + EMS weld are uniform and narrower, relatively. The measurements show that the average width of a GTAW weld is 9.765 mm with a standard deviation of 0.327, and that the one for a GTAW + EMS weld is 8.027 mm with a standard deviation of 0.262.

The surface of welds was also observed with a laser confocal microscope, as shown in Figure 4. There are strip-like structures parallel to the welding direction, which could be oxides formed during solidification. On the GTAW weld, the longest strip-like structure is about 500–600 μm and the shortest

one is about 200–300 μm. However, on the GTAW + EMS weld, the length measurements of 200–300 μm are in the majority.

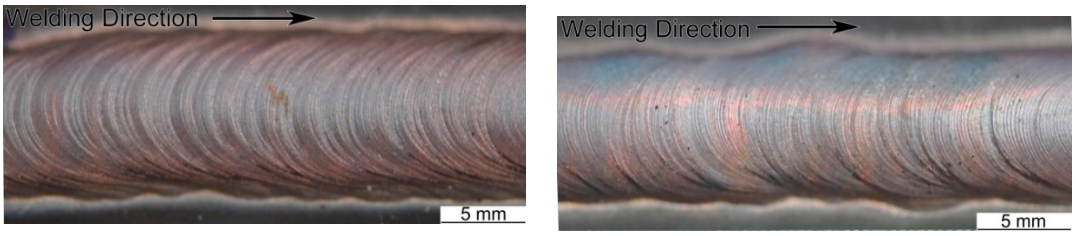

(**a**) (**b**)

Figure 3. The appearances of welds by: (**a**) gas tungsten arc welding (GTAW) and (**b**) gas tungsten arc welding (GTAW) + electromagnetic stirring (EMS).

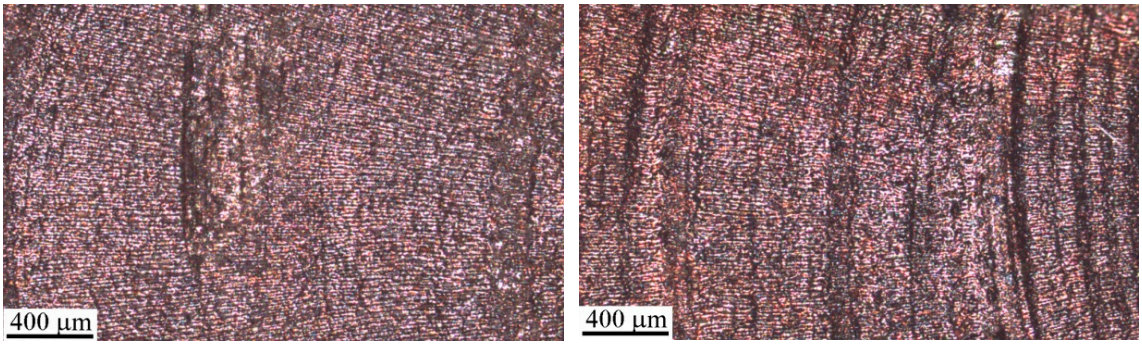

(**a**) (**b**)

Figure 4. The laser confocal microscopic images of: (**a**) GTAW and (**b**) GTAW + EMS.

The profiles of weld surfaces were further evaluated with their waviness and roughness by laser confocal microscopy. The waviness of GTAW + EMS weld is gentle, compared to the GTAW weld, as exemplified in Figure 5. It also indicates that there are two peaks and three valleys in the measured length of the GTAW weld, but that in the same measured length, there is only one valley present in the GTAW + EMS weld.

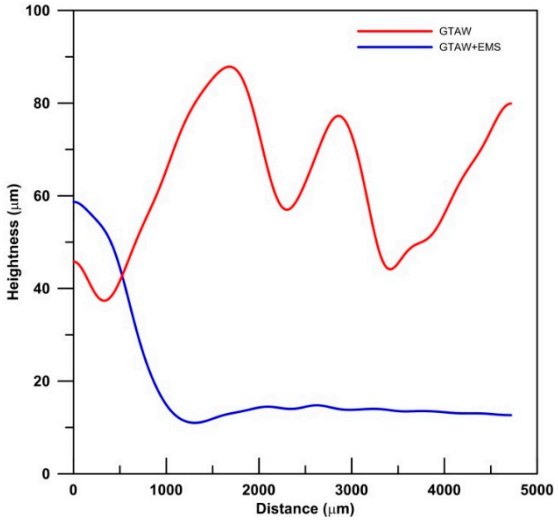

Figure 5. The waviness of weld surface.

Table 2 shows the roughness of the welds. All roughness parameters, except Rp, demonstrate that the surface of the GTAW weld is rougher than that of the GTAW + EMS weld. It implies that the application of EMS could affect the solidification of welds.

Table 2. The roughness parameters of the weld surface.

Specimen	Test	R_p (μm)	R_v (μm)	R_z (μm)	R_a (μm)	R_q (μm)
GTAW	1	37.663	28.793	66.456	6.35	8.602
	2	36.214	25.645	61.859	5.664	7.691
	3	34.798	36.278	71.076	6.355	8.707
	Average	36.225	30.239	66.464	6.123	8.333
	SD	1.433	5.462	4.609	0.398	0.559
GTAW + EMS	1	38.621	11.537	50.158	3.153	5.105
	2	35.513	11.307	46.821	2.944	4.678
	3	40.369	9.988	50.357	3.299	5.879
	Average	38.168	10.944	49.112	3.132	5.221
	SD	1.679	0.299	1.707	0.115	0.286

R_p: maximum peak height; R_v: maximum valley depth; R_z: maximum height of the profile; R_a: arithmetic mean height; R_q: squared mean height; SD: standard deviation.

3.2. The Cross-Section of Welds

Figure 6 and Table 3 show the macrographs of the cross-section and the dimensions of the welds, respectively. The dilution ratios are also given in Table 3. Obviously, the GTAW weld has larger height and width measurements than the GTAW + EMS weld. It also has a higher dilution ratio and a larger penetration-to-width ratio. However, its contact angle is smaller. These could be accounted for by a more concentrated energy generated by the GTAW process.

The inverse pole figures (IPFs) of austenitic and ferritic grains in the welds, shown in Figure 7, indicate that both the austenitic and ferritic phases have a preferred orientation [110] in the GTAW weld. On the other hand, in the GTAW + EMS weld, they do not show a preferred orientation. It suggests that EMS could prompt a more random distribution of grain orientations.

Figure 8 shows the IPF maps and the distribution of the austenitic and ferritic phases in the welds. The content of ferrite in the GTAW weld is 7.9%, while it is 2.5% in the GTAW + EMS weld. Compared with the GTAW + EMS weld, there are more ferritic phases in the GTAW weld, and the ferrite are also relatively coarser. It implies that the EMS could reduce and refine the ferritic phases in the welds.

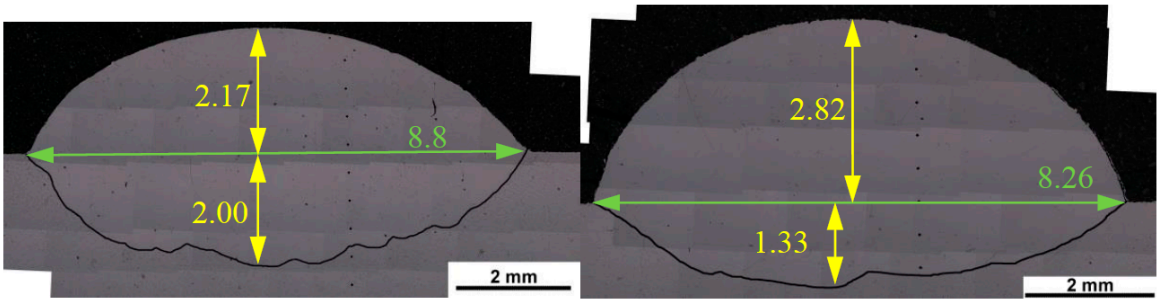

(**a**) (**b**)

Figure 6. The macrographs of the weld cross-sections by (**a**) GTAW and (**b**) GTAW + EMS.

Table 3. The dimensions of the welds.

Weld	Dilution (%)	Contact Angle	Bead Height (mm)			Bead Width (mm)	P/W
			R	P	Total		
GTAW	47.8	53–67	2.17	2.00	4.17	8.80	0.227
GTAW + EMS	30.7	74–75	2.82	1.33	4.15	8.26	0.161

R: Bead Reinforcement; P: Bead Penetration; W: Bead Width.

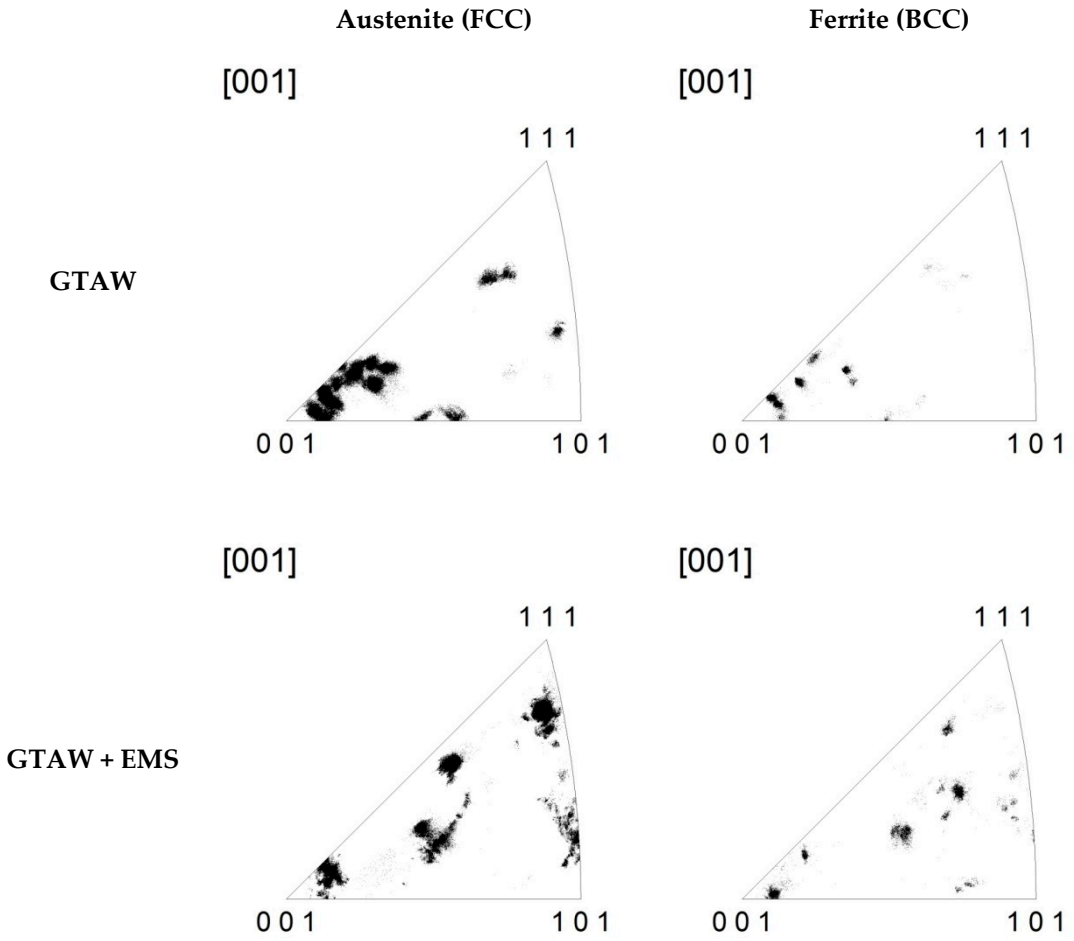

Figure 7. The inverse pole figures of austenitic and ferritic grains in the bead-on-plate (BOP) welds.

3.3. The Temperature Measurements of Welds

During BOP welding, Thermocouple #1 and Thermocouple #2 are in direct contact with the welds, indicating the temperatures of the fusion zone (FZ). On the other hand, Thermocouple #3 is not in contact with the welds, which are located about 1.8 and 1.5 mm to the fusion line of the GTAW and GTAW + EMS weldments, respectively. It registers the temperatures of the HAZs.

Figure 9 shows the temperature profiles of the welds. The surface temperature directly measured by a high-speed pyrometer is presented in Figure 9a. Figure 9b shows the internal temperature taken by Thermocouple #1. Both of them show that the GTAW + EMS weld was heated up at a higher rate and kept at the soaking temperature for a longer time than the GTAW weld. In the cooling stage from 1700 °C to 1300 °C, the GTAW + EMS weld was cooled down at a higher rate. Afterward, both welds were cooled down at similar rates.

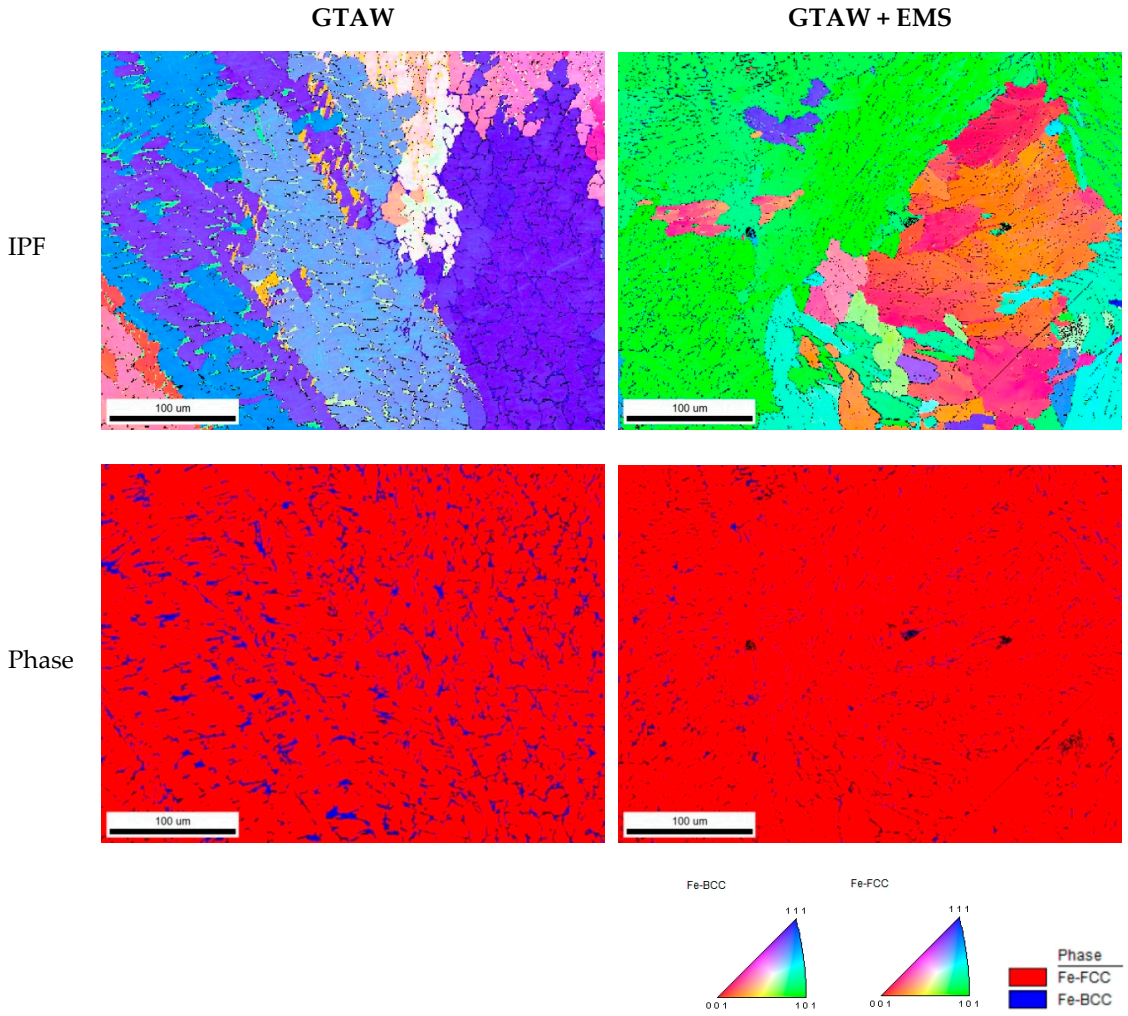

Figure 8. The inverse pole figure (IPF) maps and the distribution of austenitic and ferritic phases in the BOP welds.

Figure 10 shows the temperature profiles of the HAZs. The surface temperature, 2 mm from the FZ, was measured with a high-speed pyrometer, as shown in Figure 10a. The maximum surface temperature of the HAZ of the GTAW weldment is above 1550 °C, while that of the GTAW + EMS weldment is about 1300 °C.

The measurements of the internal temperature of HAZs are shown in Figure 10b. The temperature of HAZ of the GTAW weldment, taken by R-type thermocouple, reaches its maximum and stays at the maximum temperature for a longer period relative to the GTAW + EMS weldment. There are also distinct kinds of temperature fluctuations present throughout the welding process.

The temperature alteration rate (TAR) means the temperature difference divided by the time difference between two measuring points. Figures 11 and 12 display the relationship between the temperatures and the TARs during the heating/cooling stages of the FZs and HAZs, respectively.

The TARs of the surface temperature measured by a high-speed pyrometer is shown in Figure 11a, while Figure 11b indicates the TARs of internal temperature by the thermocouples. On the weld surface, the GTAW weldment and the GTAW + EMS weldment have similar TAR distributions. The figures show that the TARs are positive during heating and negative during cooling, except for some of the GTAW welds. These observations are in line with the general understanding of the temperature profiles during welding.

Inside the welds, most of the TARs of the GTAW weldments are positive during heating and negative during cooling. By contrast, the TARs of the GTAW + EMS weldments concurrently show

positive or negative values during the heating and cooling stages. It is noted that the TARs of the GTAW + EMS welds are larger in magnitude than those of the GTAW welds. The absolute magnitude of positive TARs is equivalent to that of negative ones at the same temperatures related to either heating or cooling.

Figure 12a shows the relationship between the temperature and the TARs of the HAZ surface. For the GTAW weldments, the TARs are higher when the temperature is above 1000 °C on heating and 1300 °C on cooling. For the GTAW + EMS weldments, they are even higher when the temperature is above 900 °C in either the heating or cooling stage, as shown in Figure 12a.

Figure 12b is different from Figure 12a, but it is similar to Figure 11b. It shows that the depth of the measuring position could affect the temperature measurement as a result of the variation of heat transfer with depth.

Considering that melting-solidification and phase transformation would occur in the FZs and HAZs of stainless steel, the TARs are analyzed further when the temperature is above 1300 °C for the FZs and 800 °C for the HAZs. Table 4 shows the results.

As for the statistic figures shown in Table 4, there are positive TARs present over around 80% of the heating stage for the GTAW weldment, but over about 50–60% of the GTAW + EMS weldment heating stage with the exception of the FZ surface with positive TARs almost throughout its heating course. On the other hand, the statistics show positive TARs occurring with about 30% and 10% of the cooling stage for the interior and the surface of the GTAW weldment respectively, and 30–47% of the cooling process for the GTAW + EMS weldment other than its FZ surface.

Table 4 shows that the occurrence percentage of positive TARs varies with the measuring position and the application of EMS. The positive TARs prevail on the heating stage, while the negative ones dominate the cooling process. In the GTAW weldments, the ratios of positive to negative TARs are more than 3, and they are less than 0.45 for the cooling process. It could result from the significant impact of the GTAW heat source.

Table 4 also suggests that EMS could facilitate maintaining the ratio of positive to negative TARs around a specific value. Both the ratios for the HAZ of the GTAW + EMS weldment on either heating or cooling are almost identical, approximating to 1. It means that the EMS increases the numbers of the TARs back and forth between positive and negative values. It also reveals that EMS could enlarge the magnitude of positive and negative TARs. The increase of the fluctuation numbers and magnitude of TARs could be the crucial factors affecting the metallurgical features of the FZ of GTAW + EMS weldment, which are different from those of the GTAW ones.

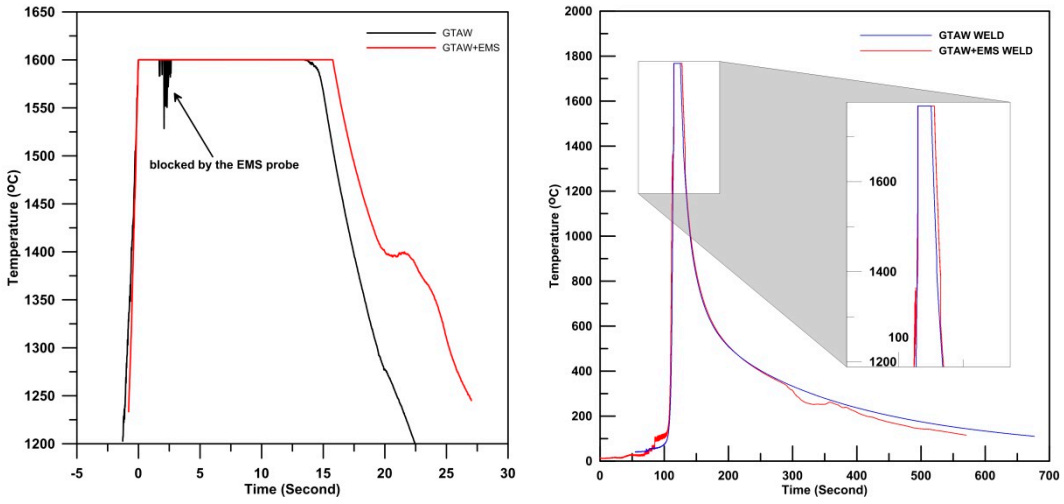

(**a**) (**b**)

Figure 9. The temperature profiles of welds: (**a**) high-speed pyrometer and (**b**) R-type thermocouple.

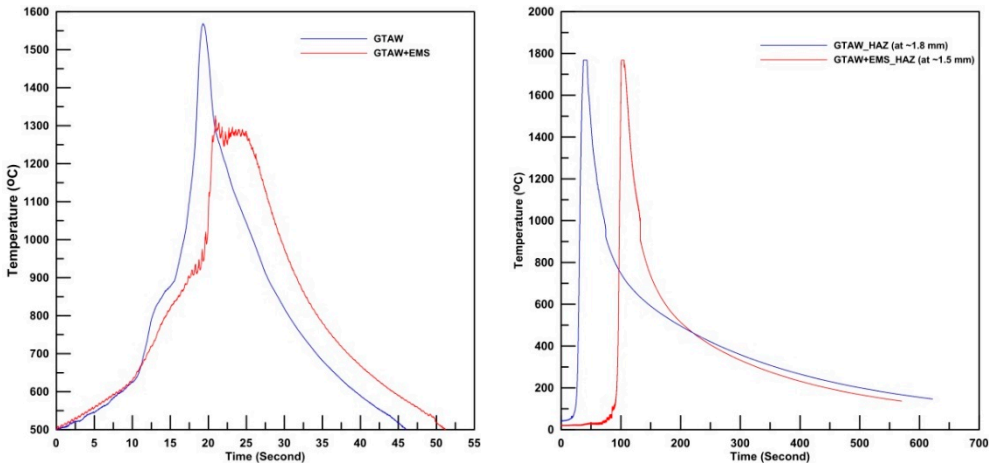

(**a**) (**b**)

Figure 10. The temperature profiles of heat-affected zones (HAZs): (**a**) high-speed pyrometer [6] and (**b**) R-type thermocouple.

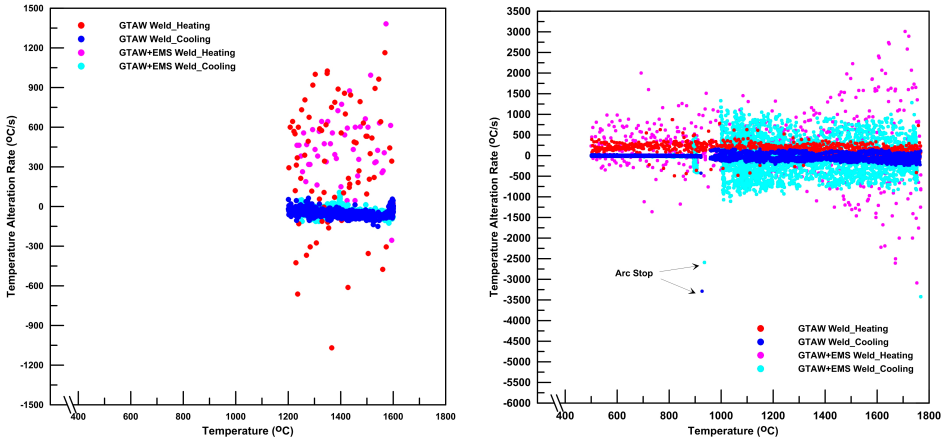

(**a**) (**b**)

Figure 11. The relationship between the temperature and the temperature alteration rates (TARs) of the fusion zone: (**a**) high-speed pyrometer and (**b**) R-type thermocouple.

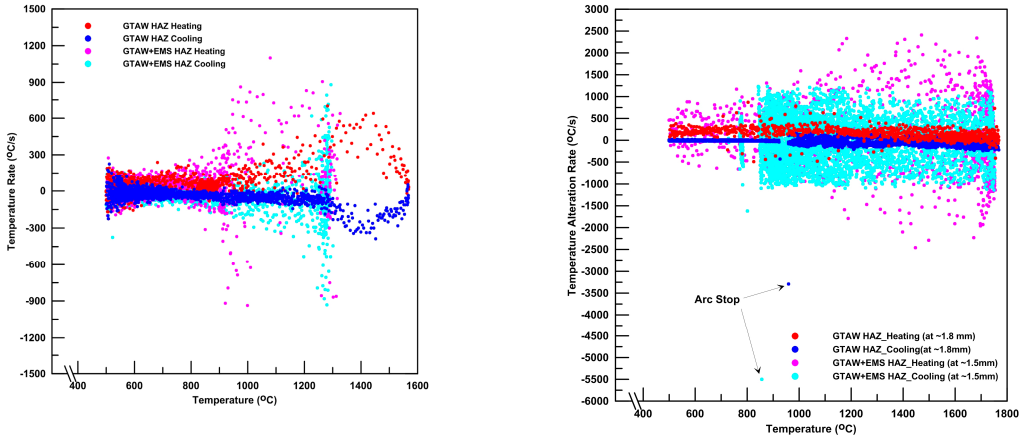

(**a**) (**b**)

Figure 12. The relationship between the temperature and the TARs of the HAZ area: (**a**) high-speed pyrometer and (**b**) R-type thermocouple.

Table 4. The statistics of temperate alteration rates.

Location	Period	Specimen		Temperature Alteration Rates (°C/s)			
				POS (%)	NEG (%)	Ratio *	Max/Min
Interior (Thermal Couple)	Heating	GTAW	FZ	83.9	13.1	6.40	730/−410
			HAZ	87.9	10.0	8.79	870/−490
		GTAW + EMS	FZ	63.8	35.7	1.79	3010/−3090
			HAZ	50.9	48.9	1.04	2410/−2460
	Cooling	GTAW	FZ	30.3	67.0	0.45	140/−240
			HAZ	22.5	64.8	0.35	160/−430
		GTAW + EMS	FZ	34.0	61.0	0.56	1330/−3420
			HAZ	47.2	52.2	0.90	1120/−1120
Surface (Pyrometer)	Heating	GTAW	FZ	76.0	24.0	3.17	1162/−1068
			HAZ	87.6	7.7	11.38	700/−81
		GTAW + EMS	FZ	97.4	2.4	40.58	1381/−256
			HAZ	60.9	35.3	1.73	1100/−937
	Cooling	GTAW	FZ	7.4	90.6	0.08	56/−150
			HAZ	1.9	95.6	0.02	50/−386
		GTAW + EMS	FZ	11.8	83.7	0.14	106/−125
			HAZ	31.3	64.4	0.49	881/−931

* Ratio = POS/NEG.

4. Discussion

According to the static flow analysis by Kuo [26], the highest temperature point is on the surface of the arc weld. There are three main active forces inside the fusion zone, i.e., buoyancy force, electromagnetic force, and surface tension force. The three forces drive the convection flow inside the weld pool to achieve heat transfer equilibrium. Among them, buoyancy and surface tension could drive the molten metal of the fusion zone to flow from the bottom to the top and from the center to the boundary. The electromagnetic force, with its direction opposite to the above two, is the leading force controlling the weld penetration.

Table 4 shows that there are positive TARs present over more than 80% of the heating stage for the GTAW weld and less than 30% of its cooling process. It implies that the TARs oscillate less between positive and negative regions during either of the heating and cooling stages. It could be accounted for by the GTAW design that the heat source (the high-temperature point) is to move along the direction of the welding path. In consequence, the convection path inside of the welding pool is relatively fixed, therby generating less internal disturbance. For the GTAW + EMS weld, for either heating or cooling, the occurrence percentage of positive TARs is close to 50%. The TARs could oscillate more frequently between positive and negative regions. When performing GTAW + EMS welding, the arc rotates around its center and moves along the welding path. The high-temperature point not only moves back and forth along the welding path but also oscillates from side to side periodically. The convection path from the high-temperature point to the inside of the welding pool changes with the progression of welding accordingly, inducing more flow disturbance inside the FZ.

The ripples of welds are related to the pressure oscillation on the FZ surface during welding [27]. The GTAW + EMS weld has denser ripples than the GTAW weld. It could result from the effect of oscillation generated by the EMS. It was reported that the arc pressure could affect the oscillation of the FZ [28,29]. When performing GTAW + EMS welding, the arc is deflected to rotate by the external electromagnetic force, which in turn agitates the welding pool. As the arc rotates, its pressure changes to increase the oscillation. The ripples of welds become denser as a result.

This study shows that EMS could reduce penetration and dilution. However, other studies show a reverse effect to increase penetration [20,30,31]. The disparity in the observations could result from the distinct setups and parameters employed. It is necessary to investigate the effects of those factors on heat transfer further.

The reduction of segregation and pores, as well as the grain refinement in the weld, are the additional benefits of EMS [4,6,9,14,32,33]. The author's previous study [8] showed that EMS could

make the grain boundaries less tortuous and the transformed austenite smaller in the HAZs. Although the temperature profiles were almost the same, GTAW welds had smaller grains with massive ferrite colonies and more precipitates. On the other hand, GTAW + EMS welds had denser ferrite colonies with multi-orientations and fewer precipitates, as shown in Figure 13. It is believed that a higher dilution leads to more impurities introduced from the base metals, i.e., the cast stainless steel. Consequently, more heterogeneous nucleation occurs in the fusion zone of the GTAW weld.

EMS could reduce the dilution to avoid the impurities induced from the base metal into the weld, which can improve the mechanical properties of the welds. This mode of EMS could refine the grains and enhance the isotropy of grains [33,34].

There are two theories about the mechanism of grain refinement by EMS. One is that the electromagnetic force could shred the dendrite tip and the secondary arm to generate more crystal embryos, thus refining the weld [4,30]. The other is that the EMS can lower the temperature gradient of the fusion zone to increase heterogeneous nucleation and thereby refine the grains [35].

During welding, EMS changes the heat transfer of the molten pool to facilitate the fluctuation of the TARs between positive and negative regions. It can prompt the solid-liquid interface of grains to move uniformly toward various directions when solidifying, which is an important factor prompting the grains to grow finer and more isotropic.

In this study, the EMS frequency set at 3 Hz was proven to be the optimal parameter for the microstructural refinement [34]. At this frequency, the ratios of positive to negative TARs for the HAZ of GTAW + EMS weldment on either heating or cooling are approximate to 1. TARs could be a useful index of microstructural refinement for setting the EMS parameters and monitoring the welding process.

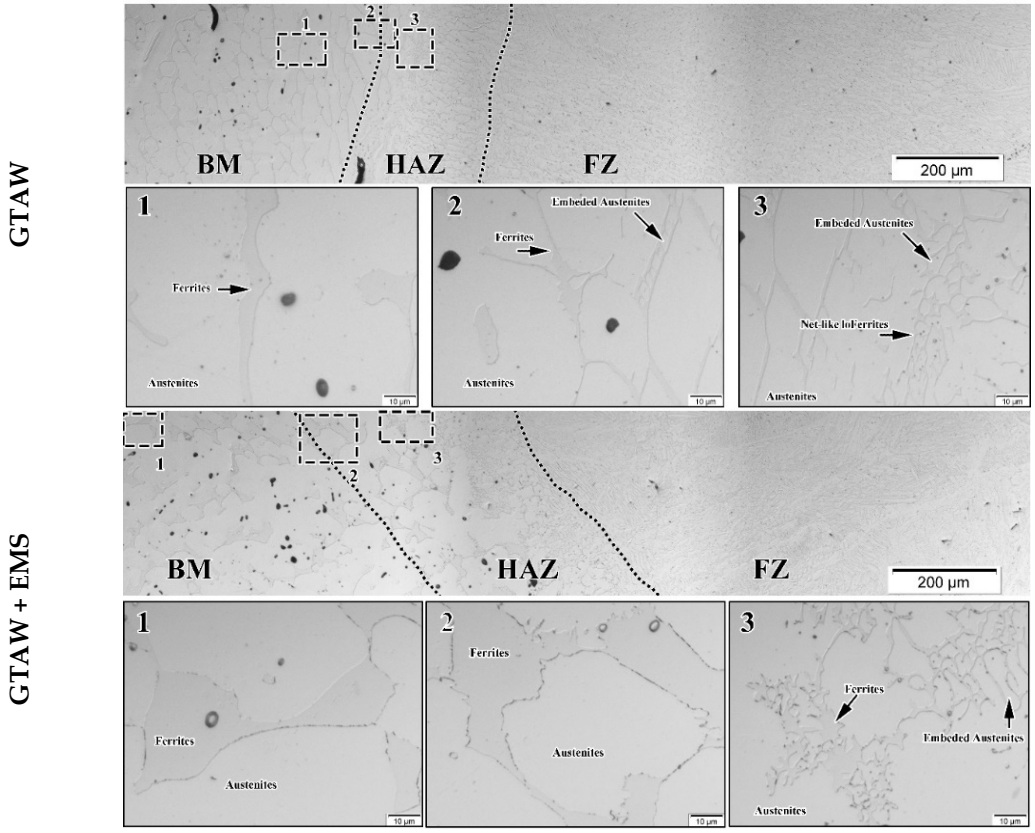

(**a**)

Figure 13. *Cont.*

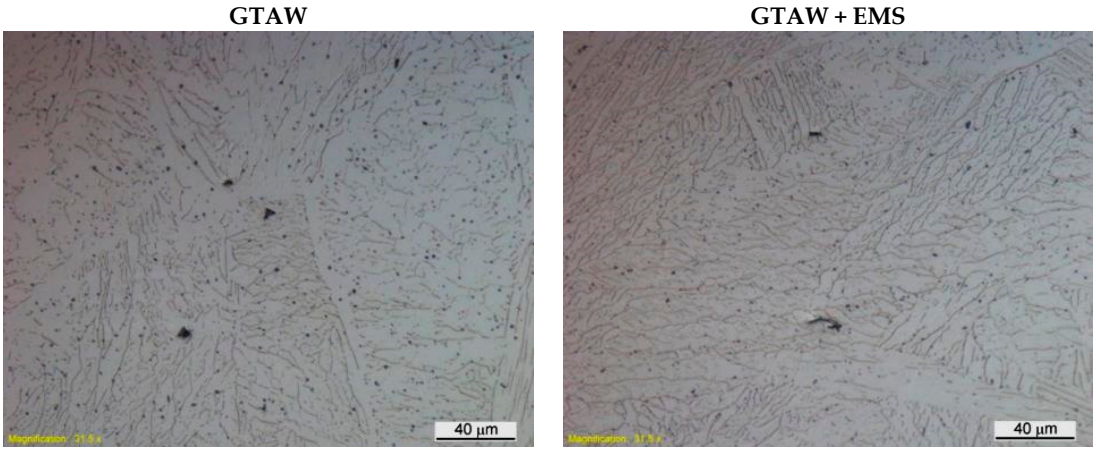

Figure 13. The optical microscope micrographs of the CF-8A butt-welds: (**a**) HAZ and (**b**) fusion zone [8].

5. Conclusions

The influence of temperature fluctuation on the appearance and microstructure of GTA stainless steel welds by electromagnetic stirring was investigated in detail. The results show that EMS can deflect the arc into rotating to facilitate temperature alteration rates (TARs) to fluctuate between positive and negative regions and increase in magnitude as well. With the increase in the fluctuation numbers and magnitude of the TARs, the weld appearance becomes denser in ripples and less in roughness. The height and width of the weld were also reduced to decrease the dilution and penetration-to-width ratios. The grains in the welds grow smaller and more isotropic.

The observations of the changes of TARs and the weld appearance by EMS imply the variations of heat transfer and the physical phenomena, e.g., arc pressure, during welding. The change of heat transfer could be a cricual factor for the grain refinement of welds.

At the frequency of 3 Hz, the ratios of positive to negative TARs for the HAZ of GTAW + EMS weldment on either heating or cooling are approximate to 1. It is thought that TARs could be a useful index of microstructural refinement for setting the EMS parameters and monitoring the welding process.

Author Contributions: Conceptualization, Methodology, Project administration, Writing—original draft, S.-L.J.; Data curation, Investigation, Formal analysis, S.-L.J., D.-P.S., and J.-T.L.; Supervision, J.-Y.H.; Validation, Writing—review and editing, S.-L.J., J.-Y.H. All authors have read and agreed to the published version of the manuscript.

Funding: This research received no external funding.

Conflicts of Interest: The authors declare no conflict of interest.

References

1. Wei, P.S. The Physics of Weld Bead Defects. In *Welding Processes*; Kovacevic, R., Ed.; IntechOpen Limited: London, UK, 2012; pp. 395–414.
2. Wang, J.; Sun, Q.; Zhang, T.; Zhang, S.; Liu, Y.; Feng, J. Arc characteristics in alternating magnetic field assisted narrow gap pulsed GTAW. *J. Mater. Process. Technol.* **2018**, *254*, 254–264. [CrossRef]
3. Kutelu, B.J.; Seidu, S.O.; Eghabor, G.I. Review of GTAW Welding Parameters. *J. Miner. Mater. Character. Eng.* **2018**, *6*, 541–554. [CrossRef]
4. Wu, H.; Chang, Y.; Lu, L.; Bai, J. Review on magnetically controlled arc welding process. *Int. J. Adv. Manuf. Technol.* **2017**, *91*, 4263–4273. [CrossRef]
5. Wu, C.; Yang, F.; Gao, J. Effect of external magnetic field on weld pool flow conditions in high-speed gas metal arc welding. *Proc. Inst. Mech. Eng. Part B J. Eng. Manuf.* **2016**, *230*, 188–193. [CrossRef]

6. Larquer, T.R.; Reis, R.P. Gas Tungsten Arc Welding with Synchronized Magnetic Oscillation. In *Joining Technologies*; Ishak, M., Ed.; IntechOpen: Rijeka, Croatia, 2016; Available online: https://www.intechopen.com/books/joining-technologies/gas-tungsten-arc-welding-with-synchronized-magnetic-oscillation (accessed on 30 October 2019).
7. Su, Y.H.; Liu, Z.J.; Liu, D. Effect of Magnetic Field on Microstructure and Properties of Magnesium Alloy Welded Joint with GTAW. *Adv. Mater. Res.* **2011**, *189*, 3507–3510. [CrossRef]
8. Jeng, S.L.; Su, D.P.; Lee, J.T.; Huang, J.Y. Effects of Electromagnetic Stirring on the Cast Austenitic Stainless Steel Weldments by Gas Tungsten Arc Welding. *Metals* **2018**, *8*, 630. [CrossRef]
9. Saini, S.; Gupta, V.; Nagpal, R.; Gupta, R.; Kuday, V. A review on the effect of magnetic field on weld quality and weld geometry in arc welding. *Int. J. Adv. Educ. Res.* **2017**, *2*, 57–63.
10. Yu, X.; Lim, Y.C.; Smith, R.; Babu, S.S.; Farson, D.F.; Lippold, J.C.; McCracken, S. Reducing hot cracking tendency of dissimilar weld overlay by magnetic arc oscillation. *Mater. Sci. Technol.* **2014**, *30*, 930–937. [CrossRef]
11. Bachmann, M.; Avilov, V.; Gumenyuk, A.; Rethmeier, M. Experimental and Numerical Investigation of an Electromagnetic Weld Pool Support System for High Power Laser Beam Welding of Austenitic Stainless Steel. *J. Mater. Process. Technol.* **2014**, *3*, 578–591. [CrossRef]
12. Ai, Y.; Jiang, P.; Wang, C.; Mi, G.; Geng, S.; Liu, W.; Han, C. Investigation of the Humping Formation in the High Power and High Speed Laser Welding. *Optics Lasers Eng.* **2018**, *107*, 102–111. [CrossRef]
13. Üstündağ, Ö.; Avilov, V.; Gumenyuk, A.; Rethmeier, M. Improvement of Filler Wire Dilution Using External Oscillating Magnetic Field at Full Penetration Hybrid Laser-Arc Welding of Thick Materials. *Metals* **2019**, *9*, 594. [CrossRef]
14. Watanabe, T.; Nakamura, H.; Ei, K. Grain refinement by TIG welding with electromagnetic stirring—A study of solidification control of austenitic stainless steel weld metal. *Weld. Int.* **1989**, *3*, 312–317. [CrossRef]
15. Lim, Y.C.; Yu, X.; Cho, J.H.; Sosa, J.D.; Farson, F.; Babu, S.S.; McCracken, S.; Flesner, B. Effect of magnetic stirring on grain structure refinement Part 2—Nickel alloy weld overlays. *Sci. Technol. Weld. Join.* **2010**, *15*, 400–406. [CrossRef]
16. Villafuerte, J.C.; Kerr, H.W. Electromagnetic Stirring and Grain Refinement in Stainless Steel GTA Welds. *Weld. J.* **1990**, *1*, 1s–13s.
17. Liu, Y.; Sun, Q.; Liu, J.; Wang, S.; Feng, J. Effect of axial external magnetic field on cold metal transfer welds of aluminum alloy and stainless steel. *Mater. Lett.* **2015**, *152*, 29–31. [CrossRef]
18. Vollertsen, F.; Thomy, C. Magnetic Stirring during Laser Welding of Aluminum. *J. Laser Appl.* **2006**, *18*, 28–34. [CrossRef]
19. Kou, S.; Le, Y. Grain Structure and Solidification Cracking in Oscillated Arc Welds of 5052 Aluminum Alloy. *Metal. Trans. A* **1985**, *16*, 1345–1352. [CrossRef]
20. Malinowski-Brodnicka, M.; Ouden, G.D.; Vink, W.J.P. Effect of Electromagnetic Stirring on GTA Welds in Austenitic Stainless Steel. *Weld. J.* **1990**, *91*, 52s–59s.
21. Sivaprasad, K.; Ganesh, S. Influence of Magnetic Arc Oscillation and Current Pulsing on Fatigue Behavior of Alloy 718 TIG Weldments. *Mater. Sci. Eng. A* **2007**, *448*, 120–127. [CrossRef]
22. Lim, Y.C.; Yu, X.; Cho, J.H.; Sosa, J.D.; Farson, F.; Babu, S.S.; McCracken, S.; Flesner, B. Effect of magnetic stirring on grain structure refinement: Part 1—Autogenous nickel alloy welds. *Sci. Technol. Weld. Join.* **2010**, *15*, 583–589. [CrossRef]
23. Bachmann, M.; Avilov, V.; Gumenyuk, A.; Rethmeier, M. About the influence of a steady magnetic field on weld pool dynamics in partial penetration high power laser beam welding of thick aluminum parts. *Int. J. Heat Mass Transf.* **2013**, *60*, 309–321. [CrossRef]
24. Wang, L.; Wu, C.; Chen, J.; Gao, J. Influence of the external magnetic field on fluid flow, temperature profile and humping bead in high speed gas metal arc welding. *Int. J. Heat Mass Transf.* **2018**, *116*, 1282–1291. [CrossRef]
25. Yudodibroto, B.Y. The Effect of Electro-Magnetic Stirring on the Weld Microstructure of Aluminum Alloys. Master's Thesis, Delft University of Technology, Delft, The Netherlands, 2000.
26. Kuo, S. *Welding Metallurgy*, 1st ed.; John Wiley & Sons: New York, NY, USA, 1987; pp. 91–99.
27. Kotecki, D.J.; Cheever, D.L.; Howden, D.G. Mechanism of Ripple Formation During Weld Solidification. *Weld. J.* **1972**, *8*, 386s–391s.

28. Xiao, Y.H.; DenOuden, G. Weld Pool Oscillation during GTA Welding of Mild Steel The oscillation behavior of the GTA weld pool depends on the welding conditions and can be used for in-process control of weld penetration. *Weld. J.* **1993**, *72*, 428s–434s.
29. Yudodibroto, B.Y.B. Liquid Metal Oscillation and Arc Behaviour during Welding. Ph.D. Thesis, Delft University of Technology, Delft, The Netherlands, 25 January 2010.
30. Nomura, K.; Ogino, Y.; Hirata, Y. Shape Control of TIG Arc Plasma by Cusp Type Magnetic Field with Permanent Magnets. *Q. J. Jpn. Weld. Soc.* **2009**, *27*, 170–175. [CrossRef]
31. Janaki Ram, G.D.; Murugesan, R.; Sundaresan, S.J. Fusion zone grain refinement in aluminum alloy welds through magnetic arc oscillation and its effect on tensile behavior. *J. Mater. Eng. Perform.* **1999**, *8*, 513–520. [CrossRef]
32. McCracken, S.; Willis, E. Welding Issues: Alloy 52 Weldability & Testing; Magnetic Stir Welding; Laser & Friction Stir Welding on Irradiated Material. In Proceedings of the NRC/Industry Technical Meeting, Rockville, MD USA, 9 June 2011; Available online: https://www.nrc.gov/docs/ML1116/ML11167A261.pdf (accessed on 30 October 2019).
33. Kung, C.Y.; Yu, G.P.; Huang, J.H.; Jeng, S.L. The effect of electromagnetic stirring on the microstructure and mechanical properties of 309L stainless steel welds. In Proceedings of the 10th International Conference on Trends in Welding Research and 9th International Welding Symposium of Japan Welding Society (9WS), Tokyo, Japan, 11–14 October 2016.
34. Kung, C.Y.; Jeng, S.L. *Effects of Magnetic-Stirring on the Austenitic Stainless Steel Welds*; INER report (INER-11704R); Institute of Nuclear Energy Research: Taoyuan, Taiwan, 2015.
35. Pearce, B.P.; Kerr, H.W. Grain refinement in magnetically stirred GTA welds of aluminum alloys. *Metall. Trans. B* **1981**, *12*, 479–486. [CrossRef]